Effects of massive neutrinos on the large-scale structure of the Universe

Federico Marulli,[1][★] Carmelita Carbone,[1,2] Matteo Viel,[3,4] Lauro Moscardini[1,2,5] and Andrea Cimatti[1]

[1]*Dipartimento di Astronomia, Alma Mater Studiorum - Università di Bologna, via Ranzani 1, I-40127 Bologna, Italy*
[2]*INAF – Osservatorio Astronomico di Bologna, Via Ranzani 1, 40127 Bologna, Italy*
[3]*INAF – Osservatorio Astronomico di Trieste, Via G. B. Tiepolo 11, I-34131 Trieste, Italy*
[4]*INFN/National Institute for Nuclear Physics, Sezione di Trieste, Via Valerio 2, I-34127 Trieste, Italy*
[5]*INFN/National Institute for Nuclear Physics, Sezione di Bologna, viale Berti Pichat 6/2, I-40127 Bologna, Italy*

ABSTRACT

Cosmological neutrinos strongly affect the evolution of the largest structures in the Universe, i.e. galaxies and galaxy clusters. We use large box-size full hydrodynamic simulations to investigate the non-linear effects that massive neutrinos have on the spatial properties of cold dark matter (CDM) haloes. We quantify the difference with respect to the concordance ΛCDM model of the halo mass function and of the halo two-point correlation function. We model the redshift-space distortions and compute the errors on the linear distortion parameter β introduced if cosmological neutrinos are assumed to be massless. We find that, if not taken correctly into account and depending on the total neutrino mass M_ν, these effects could lead to a potentially fake signature of modified gravity. Future nearly all-sky spectroscopic galaxy surveys will be able to constrain the neutrino mass if $M_\nu \gtrsim 0.6$ eV, using β measurements alone and independently of the value of the matter power spectrum normalization σ_8. In combination with other cosmological probes, this will strengthen neutrino mass constraints and help breaking parameter degeneracies.

Key words: cosmology: observations – cosmology: theory – dark matter.

1 INTRODUCTION

Neutrinos are so far the only dark matter candidates that we actually know to exist. Since deviations from the standard model in the form of extra neutrino species are still uncertain (Giusarma et al. 2011; Gonzales-Morales et al. 2011), in this paper we focus on standard neutrino families only. It is now established from solar, atmospheric, reactor and accelerator neutrino experiments that neutrinos have non-zero mass implying a lower limit on the total neutrino mass given by $M_\nu \equiv \sum m_\nu \sim 0.05$ eV (Lesgourgues & Pastor 2006), where m_ν is the mass of a single neutrino species. On the other hand the absolute masses are still unknown. Since neutrino mass affects the evolution of the Universe in several observable ways, its measurements can be obtained from different cosmological probes as observations of cosmic microwave background (CMB), galaxy clustering, Lyα forest and weak lensing data (Abazajian et al. 2011).

In particular, a thermal neutrino relic component in the Universe impacts both the expansion history and the growth of cosmic structures. Neutrinos with mass $\lesssim 0.6$ eV become non-relativistic after the epoch of recombination probed by the CMB, and this

mechanism allows massive neutrinos to alter the matter-radiation equality for a fixed $\Omega_m h^2$ (Lesgourgues & Pastor 2006). Massive neutrinos act as non-relativistic particles on scales $k > k_{nr} = 0.018(m_\nu /1\text{eV})^{1/2}\Omega_m^{1/2}$ h Mpc^{-1}, where k_{nr} is the wavenumber corresponding to the Hubble horizon size at the epoch z_{nr} when the given neutrino species becomes non-relativistic, Ω_m is the matter energy density and $h = H_0/100$ km s^{-1} Mpc^{-1}. The large velocity dispersion of non-relativistic neutrinos suppresses the formation of neutrino perturbations in a way that depends on m_ν and redshift z, leaving an imprint on the matter power spectrum for scales $k > k_{fs}(z) = 0.82H(z)/H_0/(1 + z)^2(m_\nu/1\text{ eV})$ h Mpc^{-1} (Lesgourgues & Pastor 2006; Takada, Komatsu & Futamase 2006), where neutrinos cannot cluster and do not contribute to the gravitational potential wells produced by cold dark matter and baryons. This modifies the shape of the matter power spectrum and the correlation function on these scales (see e.g. Doroshkevich et al. 1981; Hu, Eisenstein & Tegmark 1998; Abazajian et al. 2005; Kiakotou, Elgarøy & Lahav 2008; Brandbyge et al. 2010; Viel, Haehnelt & Springel 2010, and reference therein).

Massive neutrinos affect also the CMB statistics. In fact, neutrinos with mass $\lesssim 1$ eV become non-relativistic after the epoch of recombination probed by the CMB, and this mechanism alters the matter-radiation equality for a fixed $\Omega_m h^2$. *WMAP*7 alone constrains $M_\nu < 1.3$ eV (Komatsu et al. 2009) and, thanks to the

[★]E-mail: federico.marulli3@unibo.it

improved sensitivity to polarization and to the angular power spectrum damping tail, forecasts for the *Planck* satellite alone give a 1σ error on the total neutrino mass of $\sim$0.2–0.4 eV, depending on the assumed cosmological model and fiducial neutrino mass (e.g. Perotto et al. 2006; Kitching et al. 2008, and references therein). Moreover, the combination of present data sets from CMB and large-scale structure (LSS) yields an upper limit of $M_\nu < 0.3$ eV (Wang et al. 2005; Vikhlinin et al. 2009; Gonzalez-Garcia, Maltoni & Salvado 2010; Reid et al. 2010; Thomas, Abdalla & Lahav 2010). A further robust constraint on neutrino masses has been obtained using the Sloan Digital Sky Survey flux power spectrum alone, finding an upper limit of $M_\nu < 0.9$ eV (2σ confidence limit) (Viel et al. 2010). However, the tightest constraints to date in terms of a 2σ upper limit on the neutrino masses have been obtained by combining the Sloan Digital Sky Survey flux power from the Lyα forest with CMB and galaxy clustering data and result in $\Sigma m_\nu < 0.17$ eV (Seljak, Slosar & McDonald 2006). Somewhat less constraining bounds have been obtained by Goobar et al. (2006), while for forecasting on future joint CMB and Lyα constraints we refer to Gratton, Lewis & Efstathiou (2008). For further discussion on neutrino mass constraints from different probes, see e.g. Abazajian et al. (2011) and reference therein.

The forecasted sensitivity of future LSS experiments, when combined with *Planck* CMB priors, indicates that observations should soon be able to detect signatures of the cosmic neutrino background and measure the neutrino mass even in the case of the minimum mass $M_\nu = 0.05$ eV (e.g. Hannestad & Wong 2007; Kitching et al. 2008; Abell et al. 2009; Hannestad 2010; Lahav et al. 2010). In particular, Carbone et al. (2011) show that future spectroscopic galaxy surveys, such as *Euclid*, *JEDI* and *WFIRST*, not only will be able to measure the dark energy equation of state with high accuracy, but they will determine the neutrino mass scale independently of flatness assumptions and dark energy parametrization, if the total neutrino mass M_ν is >0.1 eV. On the other hand, if M_ν is <0.1 eV, the sum of neutrino masses, and in particular the minimum neutrino mass required by neutrino oscillations, can be measured in the context of a ΛCDM model.

It is therefore mandatory to measure with high accuracy the growth history of large-scale structures in order to obtain the necessary cosmological information, excluding possible systematics due to the incorrect assumption that neutrinos are massless. One way of determining the growth of structure is through the redshift-space distortions (RSD) of the galaxy distribution, caused by the line-of-sight component of galaxy peculiar velocities. RSD can be exploited in large deep redshift surveys to measure (if the galaxy bias is measured independently) the growth rate of density fluctuations $f \equiv$ d ln$D$/d ln a, with D being the linear density growth factor and $a = 1/(1 + z)$, or to measure the linear RSD parameter β (Kaiser 1987) that depends on the growth rate f and the galaxy linear bias b. In particular, β in the presence of massive neutrinos depends on both redshift and wavenumbers $\beta(z, k) = f(z, k)/b(z)$, since in this case the linear growth rate $f(z, k)$, being suppressed by free-streaming neutrinos, acquires a *scale dependence* already at the linear level (Kiakotou et al. 2008).

There are two types of RSD with competing effects acting along opposite directions on the observed galaxy correlation function. While, for large separations, large-scale bulk peculiar velocities produce a flattening effect on the correlation function and give information on the growth of structures, on small scales, random peculiar velocities cause the so-called Fingers of God (FoG), stretching compact structures along the line of sight (Scoccimarro 2004; Song & Percival 2009).

RSD have been the subject of many analyses, as reviewed in Hamilton (1998). The latest large galaxy surveys that have enabled measurements of RSD via the correlation function and the power spectrum are the two degree Field Galaxy Redshift Survey (Peacock et al. 2001; Hawkins et al. 2003; Percival et al. 2004) and the Sloan Digital Sky Survey (Tegmark et al. 2004; Zehavi et al. 2005; Tegmark et al. 2006; Okumura et al. 2008; Cabré & Gaztañaga 2009a,b). Moreover, also the VIMOS-VLT Deep Survey have been exploited in Guzzo et al. (2008) for RSD determinations from the correlation function.

Since the linear theory description is valid only at very large scales, an extension of the theoretical description has been attempted to quasi-linear and non-linear scales using empirical methods based on the so-called streaming model (Peebles 1980), consisting of linear theory and a convolution on the line of sight with a velocity distribution. This model describes the FoG elongation along the line of sight due to random motions of virialized objects (Jackson 1972). It has been shown by Guzzo et al. (2008), Cabré & Gaztañaga (2009a) and Percival & White (2009) that on quasi-linear scales a streaming model with a Gaussian velocity dispersion is a good general fit to the redshift-space power spectrum. However, this model is not accurate on very small and very large scales (Raccanelli, Samushia & Percival 2010; Taruya, Nishimichi & Saito 2010; Okumura & Jing 2011) and fitting functions based on simulation results have been used (Hatton & Cole 1999; Scoccimarro 2004; Tinker, Weinberg & Zheng 2006; Tinker 2007; Tocchini-Valentini et al. 2011). Anyway, to the purpose of this paper, the streaming model is accurate enough to robustly constrain the effect of massive neutrinos on RSD when applied on scales $\lesssim$50 h^{-1} Mpc.

In this work, we compare analytic results against a set of large N-body hydrodynamical simulations developed with an extended version of GADGET III, which is an improved version of the code described in Springel (2005), further modified to take into account the effect of massive free-streaming neutrinos on the evolution of cosmic structures (Viel et al. 2010). It is well known that galaxy/halo bias on large, linear scales is scale independent, but becomes non-linear and therefore scale dependent on smaller scales. This effect can be mimicked or enhanced by the presence of massive neutrinos. Therefore, the effect of massive neutrinos on the galaxy clustering in the quasi non-linear regime has to be explored via N-body simulations to encompass all the relevant effects, and analyse possible sources of systematic errors due to non-linearities and galaxy bias scale dependence. In particular, in this work we will focus on the DM halo mass function (MF), the DM halo bias and RSD.

The rest of the paper is organized as follows. In Section 2 we review our method and the adopted modelling of RSD. In Section 3 we describe the exploited set of N-body simulations and present our results on the neutrino effects on LSS. Finally in Section 5 we draw our conclusions.

2 FORMALISM TO MODEL REDSHIFT DISTORTIONS

2.1 Overview

In this section we describe how RSD are generated in the observed galaxy correlation function. An observed galaxy redshift is composed of the two additive terms,

$$z_{\mathrm{obs}} = z_{\mathrm{c}} + \frac{v_{\parallel}}{c}(1 + z_{\mathrm{c}}), \tag{1}$$

where z_{c} is the *cosmological* redshift, due to the Hubble flow. The second term of equation (1) is caused by galaxy peculiar velocities

where $v_\parallel$ is the component parallel to the line of sight. The *real* comoving distance of a galaxy is given by

$$r_\parallel = \int_0^{z_c} \frac{c \, dz'_c}{H(z)}, \tag{2}$$

where $H(z)$ is the so-called Hubble rate. When the distances are computed replacing z_c with z_{obs} in equation (2), i.e. without correcting for the peculiar velocity contribution, we say to be in the *redshift space*. We will refer to the redshift-space spatial coordinates using the vector s, while we will use r to indicate the real-space coordinates.

Fundamental information is hinted in the anisotropies of an observed galaxy map in redshift space. A useful statistics widely used to describe the spatial properties of a general astronomical population is the two-point correlation function, $\xi(r)$, implicitly defined as $dP_{12} = n^2[1 + \xi(r)] \, dV_1 \, dV_2$, where dP_{12} is the probability of finding a pair with one object in the volume dV_1 and the other in the volume dV_2, separated by a comoving distance r. It is convenient to decompose the distances into the two components perpendicular and parallel to the line of sight, $r = (r_\perp, r_\parallel)$, so that the correlation becomes a two-dimensional function of these variables. When measured in real space, the contour lines of $\xi(r_\perp, r_\parallel)$ are circles for an isotropic population of objects as galaxies. Instead, in redshift-space ξ is distorted: at small scales ($\lesssim 1 \, h^{-1}$ Mpc) the distortion is caused by the random motions of galaxies moving inside virialized structures. This motion changes the shape of ξ in the direction parallel to the line of sight, producing the observed FoG. At large scales the coherent bulk motion of virializing structures squashes the correlation function ξ perpendicularly to the line of sight.

A different kind of distortion, called *geometrical* or Alcock–Paczynski (AP) distortion (Alcock & Paczynski 1979), can be present if the cosmological parameters assumed in equation (2) are not the same as the true cosmological model of the Universe. In what follows, we will not consider this effect since massive neutrinos do not produce a geometrical distortion if the present-day total matter energy density parameter Ω_m is held fixed.

2.2 Modelling the dynamical distortions

At large scales and in the plane-parallel approximation, the dynamical distortions can be parameterized in the Fourier space as follows:

$$P(k) = (1 + \beta\mu^2)^2 P_{lin}(k), \tag{3}$$

where $P_{lin}(k)$ is the linear power spectrum of the matter density fluctuations and μ is the cosine of the angle between k and the line of sight. Fourier transforming equation (3) gives

$$\xi(s, \mu) = \xi_0(s)P_0(\mu) + \xi_2(s)P_2(\mu) + \xi_4(s)P_4(\mu), \tag{4}$$

where the functions P_l represent the Legendre polynomials (Hamilton 1992). The multipoles $\xi_n(s)$, $n = 0, 2, 4$, can be written as follows:

$$\xi_0(s) = \left(1 + \frac{2\beta}{3} + \frac{\beta^2}{5}\right)\xi(r), \tag{5}$$

$$\xi_2(s) = \left(\frac{4\beta}{3} + \frac{4\beta^2}{7}\right)[\xi(r) - \overline{\xi}(r)], \tag{6}$$

$$\xi_4(s) = \frac{8\beta^2}{35}\left[\xi(r) + \frac{5}{2}\overline{\xi}(r) - \frac{7}{2}\overline{\overline{\xi}}(r)\right], \tag{7}$$

where $\xi(r)$ is the real-space correlation function, and the *barred* correlation functions are defined as

$$\overline{\xi}(r) = \frac{3}{r^3}\int_0^r dr'\xi(r')r'^2, \tag{8}$$

$$\overline{\overline{\xi}}(r) = \frac{5}{r^5}\int_0^r dr'\xi(r')r'^4. \tag{9}$$

Equation (4) can be used to approximate the correlation function at large scales. To include in the model also the small scales, as discussed in Section 1, we adopt the streaming model and use the following formula

$$\xi(s_\perp, s_\parallel) = \int_{-\infty}^{\infty} dv f(v)\xi(s_\perp, s_\parallel - v/H(z)/a(z)), \tag{10}$$

where $f(v)$ is the distribution function of random pairwise velocities that are measured in physical (not comoving) coordinates (but see e.g. Matsubara 2004; Scoccimarro 2004). In this work, we adopt for $f(v)$ the form

$$f(v) = \frac{1}{\sigma_{12}\sqrt{2}}\exp\left(-\frac{\sqrt{2}|v|}{\sigma_{12}}\right), \tag{11}$$

where σ_{12} is the dispersion in the pairwise peculiar velocities.

3 THE ADOPTED SET OF NUMERICAL SIMULATIONS

The set of simulations we consider in this work have been performed by Viel et al. (2010) with the hydrodynamical tree particle mesh–smoothed particle hydrodynamics (TreePM–SPH) code GADGET III, which is an improved and extended version of the code described in Springel (2005). This code has been modified in order to simulate the evolution of the neutrino density distribution. The cosmological model adopted in the simulations is based on cold dark matter and assumes the presence of the cosmological constant (ΛCDM): $n_s = 1$, $\Omega_m = 0.3$, $\Omega_b = 0.05$, $\Omega_\Lambda = 0.7$ and $h = 0.7$ ($H_0 = 100 \, h$ km s^{-1}), plus a cosmological massive neutrino component $\Omega_\nu \equiv M_\nu/(h^2 93.8 \, \text{eV})$ (ΛCDM+ν). In what follows, we consider only the so-called 'grid-based implementation' of the simulations developed by Viel et al. (2010), where neutrinos are treated as a fluid (see also Brandbyge & Hannestad 2009, 2010). In this implementation the linear growth of the perturbations in the neutrino component is followed by interfacing the hydrodynamical code with the public available Boltzmann code CAMB[1] (Lewis, Challinor & Lasenby 2000). More specifically, the power spectra of the neutrino density component are interpolated in a table produced via CAMB of 100 redshifts in total, spanning logarithmically the range $z = 0$–49. The gravitational potential is calculated at the mesh points and the neutrino contribution is added when forces are calculated by differentiating this potential.

In this approach the gravitational force due to neutrinos is calculated based on the linearly evolved density distribution of the neutrinos in Fourier space. This implementation has the advantage that it does not suffer from significant shot noise on small scales, yielding therefore higher accuracy at scales and redshifts where the effect of the non-linear neutrino evolution is still moderate, especially for small neutrino masses. Further advantages of such a grid-based approach, aside from eliminating the Poisson noise, are the reduced requirements with regard to memory (there are no

---

[1] http://camb.info/

neutrino positions and velocities to be stored) and computational time.

The initial conditions of this set of simulations were generated based on linear matter power spectra separately computed for each component (dark matter, gas and neutrinos) with CAMB. The total matter power spectrum was normalized such that its amplitude (expressed in terms of σ_8) matches the CAMB prediction at the same redshift. The mass per simulation particle at our default resolution is 1.4×10^{10} and $6.9 \times 10^{10} \, M_{\odot} \, h^{-1}$ for gas and dark matter, respectively. In this work we consider the set of simulations with a box of comoving volume $V = (512 \, h^{-1} \, \mathrm{Mpc})^3$, and total neutrino mass $M_\nu = 0, 0.3, 0.6$ eV, respectively.

To identify DM haloes and their substructures we have used two different algorithms: a standard friends-of-friends (FOF) group finder with linking length $b = 0.2$, and the SUBFIND algorithm described in Springel et al. (2001). Apart from the right-hand panel of Fig. 1, all the results presented in this paper have been obtained using our subhalo catalogues, composed of the gravitationally bound substructures that SUBFIND identifies in each FOF haloes. However, as we have explicitly verified, all the main conclusions of this work do not change if we consider the halo catalogues instead. This happens because, as shown by Giocoli et al. (2010), in the mass range considered in this work the total MF of haloes and sub-haloes is manly dominated by the halo systems. At $z = 0$ the sub-halo contribution start to be seen only for masses $\lesssim 10^{10} \, M_{\odot} \, h^{-1}$. For all the considered M_ν values, we have restricted our analysis in the mass range $M_{\mathrm{min}} < M < M_{\mathrm{max}}$, where $M_{\mathrm{min}} = 2 \times 10^{12} \, M_{\odot} \, h^{-1}$ and $M_{\mathrm{max}} = 2 \times 10^{15}, 5 \times 10^{14}, 3 \times 10^{14}, 10^{14} \, M_{\odot} \, h^{-1}$ at $z = 0, 0.66, 1, 2$, respectively.

4 RESULTS

In this section we show how the halo MF, the halo bias and the linear RSD parameter β get modified with respect to the standard ΛCDM case, when a massive neutrino component is taken correctly into account. In particular we compare the results between the ΛCDM and the ΛCDM$+\nu$ cosmologies, and analyse if our findings agree with analytical predictions in the literature.

4.1 The halo mass function

As mentioned in Section 1, the free streaming of non-relativistic neutrinos contrasts the gravitational collapse which is the basis of cosmic structure formation. The first consequence of this mechanism is represented by a significant suppression in the average number density of massive structures. This effect can be observed in the high mass tail of the halo MF as measured from our set of simulations, and shown by the data points in the left-hand panel of Fig. 1. For a fixed amplitude of the primordial curvature perturbations $\Delta_{\mathcal{R}}^2$, the amount of the number density suppression depends on the value of the total neutrino mass M_ν. From the comparison of the corresponding MFs, we recover what is theoretically expected, i.e. the higher the neutrino mass is, the larger the suppression in the comoving number density of DM haloes becomes. The suppression affects mainly haloes of mass $10^{14} < M < 10^{15} \, M_{\odot} \, h^{-1}$, depending slightly on the redshift z. This result is in agreement with the findings of Brandbyge et al. (2010). In the same plot, we compare the measured MFs with the analytical predictions of Sheth & Tormen (2002) (ST), represented by the solid, dotted and dashed curves,
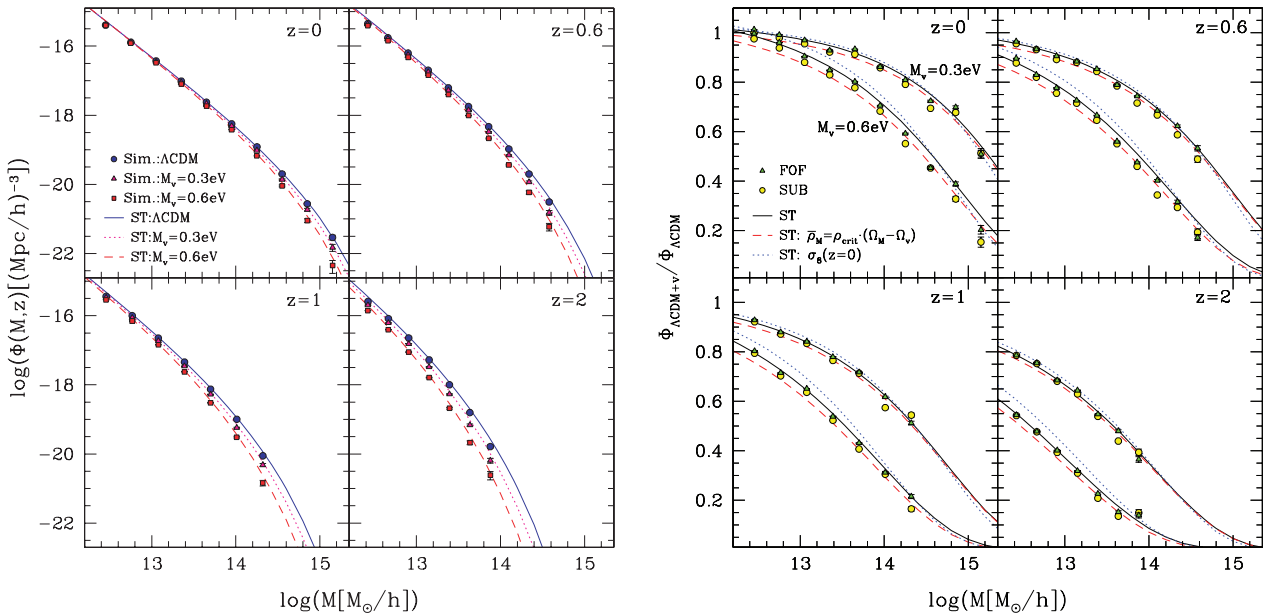

Figure 1. DM halo MF as a function of M_ν and redshift. Left: MF of the SUBFIND haloes in the ΛCDM N-body simulation (blue circles) and in the two simulations with $M_\nu = 0.3$ eV (magenta triangles) and $M_\nu = 0.6$ eV (red squares). The blue, magenta and red lines show the halo MF predicted by Sheth & Tormen (2002), where the variance in the density fluctuation field, $\sigma(M)$, for the three cases, $M_\nu = 0, 0.3, 0.6$ eV, has been computed using the linear matter $P(k)$ extracted from CAMB. Right: ratio between the halo MFs of the simulations with and without neutrinos. The green triangles show the MF ratios of the FOF haloes, while yellow circles show the ones of the SUBFIND haloes. The lines represent the ST–MF ratios: the black solid lines are the MF ratios predicted for $M_\nu = 0.3$ and 0.6 eV; the red dashed lines are the same ratios but assuming $\bar{\rho} = \rho_c(\Omega_{\mathrm{m}} - \Omega_\nu)$ in the ST–MF formula (equation 12) (Brandbyge et al. 2010); finally, the blue dotted lines are the ratios between the ST MFs in two ΛCDM cosmologies, which differ for the σ_8 normalization, as explained in the text. The error bars represent the statistical Poisson noise.

corresponding to the values $M_\nu = 0, 0.3, 0.6\,\text{eV}$, respectively. The ST fit is based on the fact that the halo MF can be written as (Press & Schechter 1974)

$$\frac{M\,\mathrm{d}M}{\bar\rho}\frac{\mathrm{d}n(M,z)}{\mathrm{d}M} = \zeta f(\zeta)\frac{\mathrm{d}\zeta}{\zeta}, \qquad (12)$$

with $\zeta \equiv [\delta_{sc}(z)/\sigma(M)]^2$, where $\delta_{sc}(z) = 1.686$ is the overdensity required for spherical collapse at z in a ΛCDM cosmology, and $\bar\rho = \Omega_m\rho_c$, where ρ_c is the critical density of the Universe. Here $\Omega_m = \Omega_{c\,dm} + \Omega_b + \Omega_\nu$, and $\mathrm{d}n(M,z)$ is the number density of haloes in the mass interval M to $M + \mathrm{d}M$. The variance of the linear density field, $\sigma^2(M)$, is given by

$$\sigma^2(M) = \int \mathrm{d}k \frac{k^2 P_{\text{lin}}(k)}{2\pi^2}|W(kR)|^2, \qquad (13)$$

where the top-hat window function is $W(x) = (3/x^3)(\sin x - x\cos x)$, with $R = (3M/4\pi\bar\rho)^{1/3}$.

The ST fit to $\zeta f(\zeta)$ is

$$\zeta f(\zeta) = A\left(1 + \frac{1}{\zeta'^p}\right)\left(\frac{\zeta'}{2}\right)^{1/2}\frac{\mathrm{e}^{-\zeta'/2}}{\sqrt\pi}, \qquad (14)$$

with $\zeta' = 0.707\zeta$, $p = 0.3$ and $A = 0.3222$ determined from the integral constraint $\int f(\zeta)\,\mathrm{d}\zeta = 1$.

In Fig. 1 the variance of the density field, $\sigma^2(M)$, has been computed with the matter power spectrum extracted from CAMB (Lewis et al. 2000), using the same cosmological parameters of the simulations. In particular, in the left-hand panel we show the MF of substructures identified using the SUBFIND algorithm, where the normalization of the matter power spectrum is fixed by $\Delta_{\mathcal{R}}^2(k_0) = 2.3 \times 10^{-9}$ at $k_0 = 0.002\,\text{Mpc}^{-1}$ (Larson et al. 2011), chosen to have the same value both in the ΛCDM$+\nu$ and in the ΛCDM cosmologies. The error bars represent the statistical Poisson noise.

In the right-hand panel of Fig. 1 we show the ratios between the halo MFs evaluated in the ΛCDM$+\nu$ and ΛCDM cosmologies. In particular, the triangles represent the ratios of the halo MFs measured directly from the simulations after identifying the structures via a FOF group finder (Springel 2005), and the filled circles represent the ratios between the ΛCDM$+\nu$ and ΛCDM MFs for the substructure evaluated via the SUBFIND algorithm.
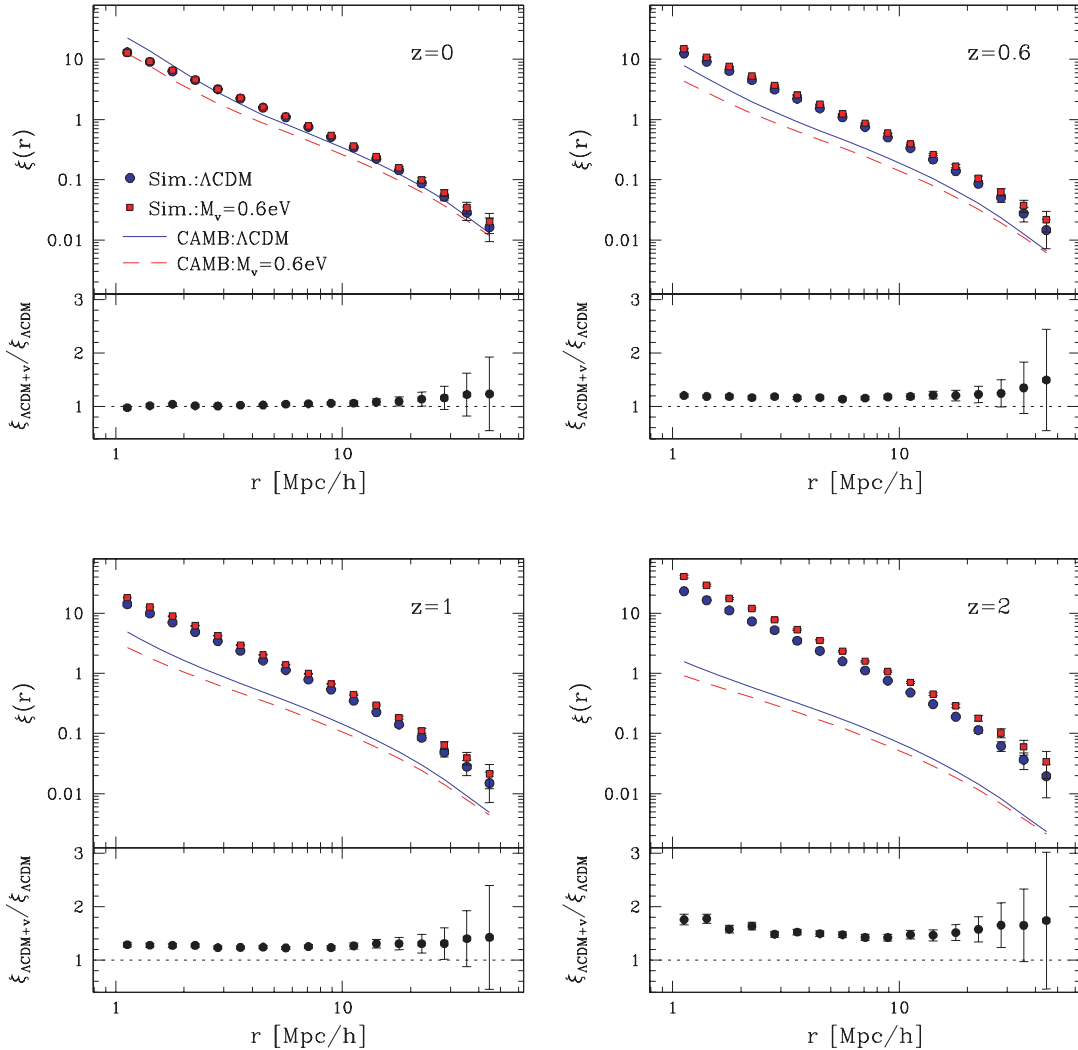

Figure 2. Real-space two-point autocorrelation function of the DM haloes in the ΛCDM N-body simulation (blue circles) and in the simulation with $M_\nu = 0.6\,\text{eV}$ (red squares). The blue and red lines show the DM correlation function, for $M_\nu = 0$ and $0.6\,\text{eV}$, respectively, obtained by Fourier transforming the non-linear power spectrum extracted from CAMB (Lewis & Bridle 2002) which exploits the HALOFIT routine (Smith et al. 2003). The bottom panels show the ratio between the halo correlation function of the simulations with and without neutrinos. The error bars represent the statistical Poisson noise corrected at large scales as prescribed by Mo, Jing & Boerner (1992).

The curves in the panel show the corresponding ST predictions for three cases: (i) the solid lines represent the ratios between the theoretical MFs when the total $\Omega_m = \Omega_{cdm} + \Omega_b + \Omega_\nu$ is inserted in equation (12) through the expression $\bar{\rho} = \Omega_m \rho_c$; (ii) the dashed lines represent the theoretical MF ratios when the quantity $\bar{\rho} = (\Omega_{cdm} + \Omega_b)\rho_c$ is used in equation (12); (iii) finally, the dotted lines represent the ratios between the ST MFs in two ΛCDM cosmologies, which differ for the σ_8 normalization, i.e. the ratio between the MF in a ΛCDM cosmology having the same σ_8 value of the simulations with a massive neutrino component, and the MF in a ΛCDM cosmology having a σ_8 value in agreement with the CMB normalization $\Delta^2_{\mathcal{R}}(k_0) = 2.3 \times 10^{-9}$ and in the absence of massive neutrinos.

We note that the MFs of the haloes obtained with the FOF algorithm look to be better fitted by the theoretical predictions of case (i), while the MFs of the substructures obtained with the SUBFIND algorithm have a trend much more similar to the predictions of case (ii) (Brandbyge et al. 2010). Moreover, we see that, as the redshift increases, the suppression of the halo number density due massive neutrinos moves also towards masses $M \leq 10^{14}\,M_\odot\,h^{-1}$. As an example, the number density of haloes with mass $10^{14}\,M_\odot\,h^{-1}$ at $z = 0$ decreases by $\sim$15 per cent for $M_\nu = 0.3\,$eV and by $\sim$30 per cent for $M_\nu = 0.6\,$eV, and, at $z = 1$, by $\sim$40 and $\sim$70 per cent, respectively.

As already discussed in Viel et al. (2010), the free-streaming of massive neutrinos leads to the well-known degeneracy between the values of σ_8 and M_ν. However, as the case (iii) lines show, the difference between the MFs with and without neutrinos does not reduce merely to a σ_8 renormalization of the background cosmology, since, even renormalizing to the same σ_8, neutrinos free-streaming alters the MF, changing its shape and amplitude especially for the less massive objects (compare the dotted-blue and solid-black lines in the right-hand panel of Fig. 1). However, the possibility to measure this effect and break the M_ν–σ_8 degeneracy depends on the value of the neutrino mass and on the sensitivity in measuring the MF at masses $M < 10^{14}\,M_\odot\,h^{-1}$. The resolution limits of our simulations do not allow us to study the properties of haloes with masses $M \lesssim 10^{12}\,M_\odot\,h^{-1}$. Future galaxy surveys, like *Euclid*, should be able to break this degeneracy measuring the number counts of low-mass galaxies together with the overall shape of the matter power spectrum (see e.g. Carbone et al. 2011). Moreover, even with present observational data it has already been possible to break the M_ν–σ_8 degeneracy. For instance, Viel et al. (2010) robustly constrained the neutrino masses using the Sloan Digital Sky Survey flux power spectrum alone, without CMB priors on σ_8.

4.2 The halo clustering and bias

As well known, massive neutrinos strongly affect also the spatial clustering of cosmic structures. As explained in Section 2.2, a standard statistics generally used to quantify the clustering degree of a population of sources is the two-point autocorrelation function. Although the free-streaming of massive neutrinos causes a suppression of the matter power spectrum on scales k larger than the neutrino free-streaming scale k_{fs}, the halo bias results to be significantly enhanced. This effect can be physically explained thinking that, starting from the same $\Delta^2_{\mathcal{R}}(k_0)$ as initial condition, due to the suppression of massive neutrino perturbations, the same halo bias would correspond, in a ΛCDM cosmology without neutrinos, to more massive haloes, which, as well known, are typically more clustered.

In fact, Fig. 2 shows, at different redshifts, the two-point DM halo correlation function measured using the Landy & Szalay (1993)
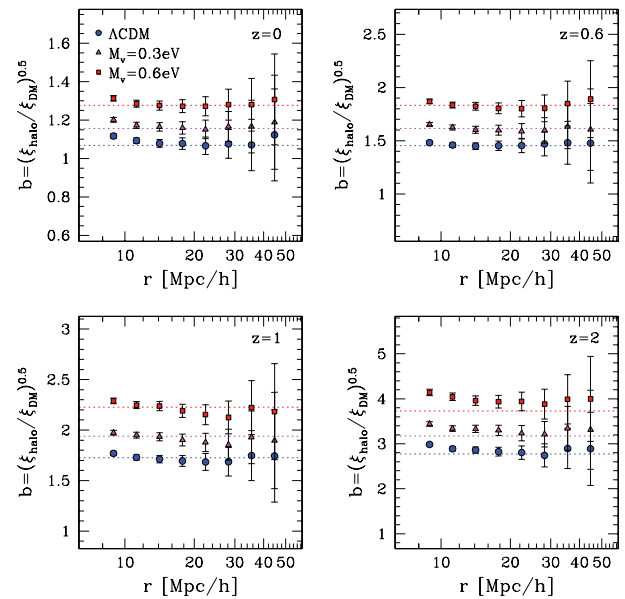

Figure 3. DM halo bias, $b = (\xi_{halo}/\xi_{DM})^{0.5}$, measured from the ΛCDM simulations (blue circles) and from the two simulations with $M_\nu = 0.3\,$eV (magenta triangles) and $M_\nu = 0.6\,$eV (red squares). The error bars represent the propagated Poisson noise corrected at large scales as prescribed by Mo et al. (1992). Dotted lines are the theoretical predictions of Sheth, Mo & Tormen (2001) (equation 15). The four panels show the results at different redshifts, as labelled.
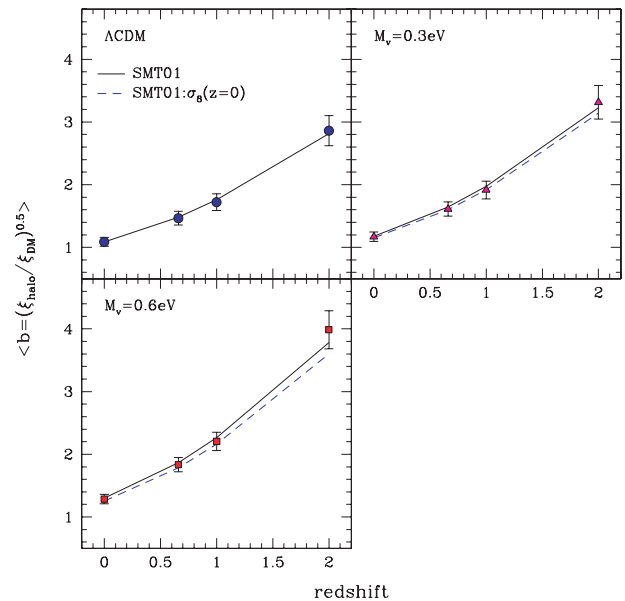

Figure 4. Mean bias (averaged in $10 < r < 50\,h^{-1}$ Mpc) as a function of redshift compared to the theoretical predictions of Sheth et al. (2001) (dotted lines) (equation 15). Here the dashed lines represent the theoretical expectations for a ΛCDM cosmology renormalized with the σ_8 value of the simulations with a massive neutrino component. The error bars represent the propagated Poisson noise corrected at large scales as prescribed by Mo et al. (1992).

estimator, compared to the correlation function of the matter density perturbations. We observe that, while for a fixed $\Delta^2_{\mathcal{R}}(k_0)$, due to neutrino free-streaming, the total matter correlation function decreases with respect to the ΛCDM case, especially on small scales (compare

the solid-blue and dashed-red lines in Fig. 2), the halo correlation function undergoes the opposite trend (compare the data points in Fig. 2), so that the matter perturbation suppression is in some way compensated by a stronger spatial clustering of the massive haloes.

In particular, the halo clustering difference between the ΛCDM and ΛCDM+ν cosmologies increases with the redshift (as it happens also for the halo MFs). For $M_\nu = 0.6\,\mathrm{eV}$ we find that the halo correlation function in the presence of massive neutrinos at $z = 1$ is ∼20 per cent larger than in a pure ΛCDM model, and at $z = 2$ the difference rises up to ∼40 per cent (see the bottom panels of Fig. 2).

This effect is even more evident in Figs 3 and 4, that show the effective bias measured from the simulations (symbols) compared to the analytical predictions (dotted lines), obtained using the Sheth et al. (2001) (SMT) bias, weighted with the ST MF of equation (12):

$$b(z) = \frac{\int_{M_{\min}}^{M_{\max}} n(M, z) b_{\mathrm{SMT}}(M, z)\, \mathrm{d}M}{\int_{M_{\min}}^{M_{\max}} n(M, z) \mathrm{d}M}, \tag{15}$$

where $M_{\min}$ and $M_{\max}$ have been defined in Section 3. Also in this case, the theoretical expectations reproduce correctly the numer-

ical findings, inside the statistical errors, and, as in the ΛCDM cosmology, the halo bias results to be scale independent on large scales, while the effect of non-linearities starts to be important for separations $r < 20\, h^{-1}$ Mpc.

4.3 Redshift-space distortions

As it happens for the halo MFs and clustering, also RSD are strongly affected by free-streaming neutrinos. Fig. 5 shows the real and redshift-space correlation functions of DM haloes extracted from the simulations as a function of the neutrino mass. In the presence of massive neutrinos the rms of galaxy peculiar velocities is smaller than in a pure ΛCDM cosmology, due to the suppression of both the growth rate $f(k, z)$ and the matter power spectrum $P(k, z)$, which enter the bulk flow predicted by linear theory (Elgarøy & Lahav 2005; Kiakotou et al. 2008):

$$\langle v^2(R_*)\rangle = (2\pi^2)^{-1}\, H_0^2 \int \mathrm{d}k f^2 P_{\mathrm{lin}}(k) W_{\mathrm{G}}^2(k R_*), \tag{16}$$

where $W_{\mathrm{G}}(k R_*)$ is the window function, e.g. for a Gaussian sphere of radius R_*, $W(k R_*) \equiv \exp(-k^2 R_*^2/2)$. This effect competes with
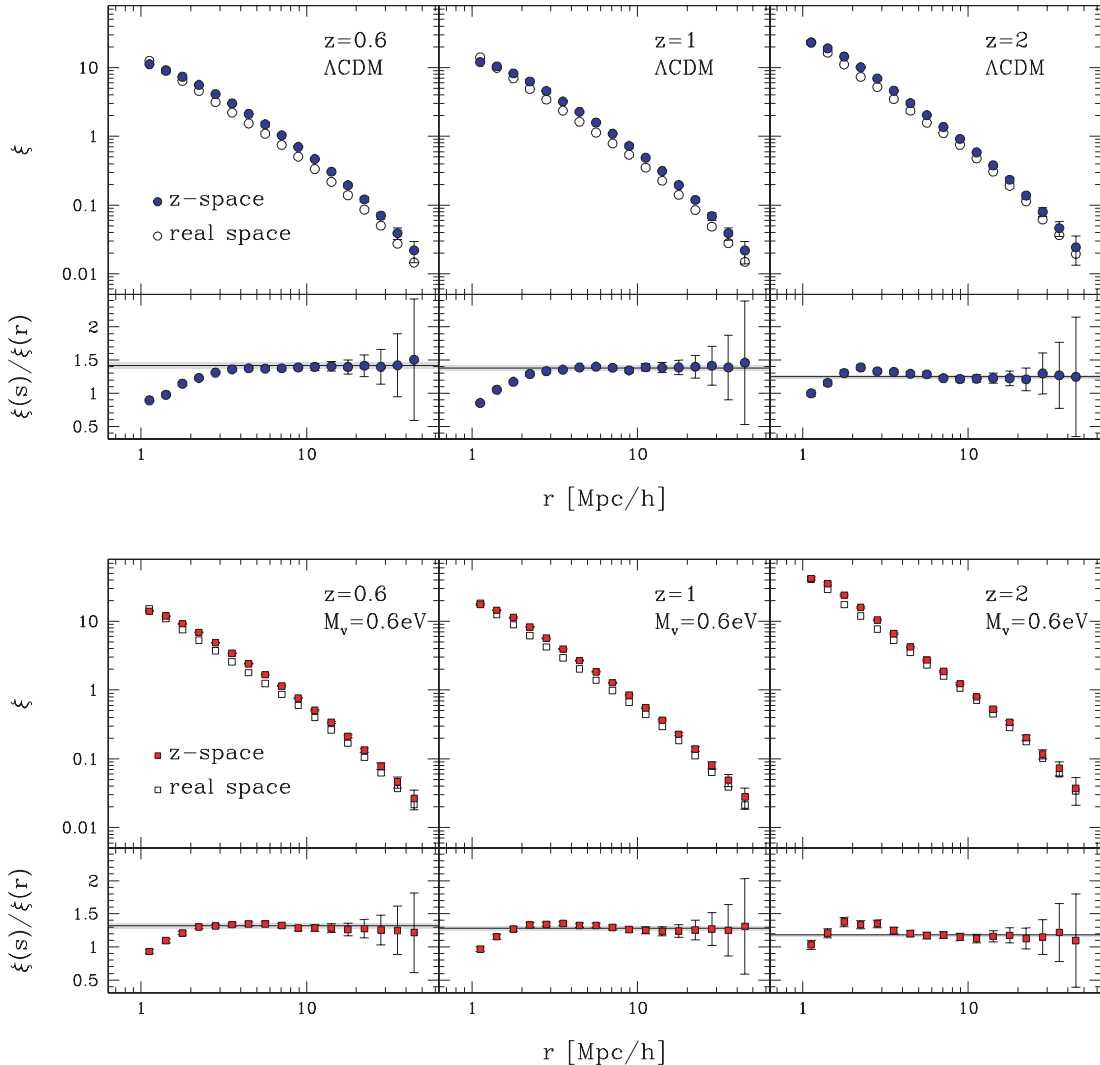

Figure 5. Two-point autocorrelation function in real and redshift space of the DM haloes in the ΛCDM *N*-body simulation (blue circles) and in the simulation with $M_\nu = 0.6\,\mathrm{eV}$ (red squares). The bottom panels show the ratio between them, compared with the theoretical expectation given by equation (17). The error bars represent the statistical Poisson noise corrected at large scales as prescribed by Mo et al. (1992).

the increase of the halo bias discussed in Section 4.2, resulting in a redshift-space halo correlation function slightly suppressed in a ΛCDM+ν cosmology. In the bottom panels of Fig. 5 we show the ratios $\xi(s)/\xi(r)$ compared to the theoretical values represented by the large-scale limit of equation (4):

$$\frac{\xi(s)}{\xi(r)} = 1 + \frac{2\beta}{3} + \frac{\beta^2}{5}. \tag{17}$$

The effect of massive neutrinos on RSD is evident in particular when the correlation function is measured as a function of the two directions perpendicular and parallel to the line of sight. In fact, from the top and bottom panels of Fig. 6, we observe that, in the case of massive neutrinos, the spatial halo clustering is less enhanced in redshift space than in real space. On large scales, this effect is due to the lower value of $\langle v^2(R_*)\rangle$ when neutrinos free-streaming is taken into account. On small scales, our analysis shows that also FoG get decreased in the presence of massive neutrinos, so that the best-fitting values of β and σ_{12}, derived by modelling galaxy clustering anisotropies, result to be different than what expected in a ΛCDM cosmology. This might induce a bias in the inferred growth rate from data analysis, and therefore a potentially false signature of modified gravity (see e.g. Simpson, Jackson & Peacock 2011). Moreover, estimates of β and σ_{12}, when compared with the ΛCDM expectations, yield an indirect neutrino mass measurement and may help breaking degeneracies with the other cosmological parameters.

We quantify these effects in Fig. 7, which shows the best-fitting values of β and σ_{12} as a function of M_ν and z, where we have neglected their scale dependence which, for the neutrino masses considered in this work, is small enough that statistical errors hide deviations of β and σ_{12} from spatial uniformity (Kiakotou et al. 2008). Therefore, in this case we have considered the linear RSD parameter as a function of the redshift alone, $\beta = f(z)/b(z) \simeq \Omega_m(z)^\gamma/b(z)$, with $\gamma = 0.545$. The data points of Fig. 7 show that neutrinos free-streaming suppresses β and σ_{12} by an amount which

increases with M_ν and z, and, fixed $\Delta^2_{\mathcal{R}}(k_0)$, is clearly distinguishable from the corresponding ΛCDM values (dashed lines). As an example, at $z = 0.6$ the β best-fitting values decrease by ~ 10 per cent for $M_\nu = 0.3$ eV, and by ~ 25 per cent for $M_\nu = 0.6$ eV. Likewise, the σ_{12} best-fitting values decrease by ~ 25 per cent for $M_\nu = 0.3$ eV, and by ~ 45 per cent for $M_\nu = 0.6$.

On the other hand, the β best-fitting values fall in the shaded grey bands, which represent the propagated ~ 10 per cent theoretical bias error. These bands contain also the theoretical predictions obtained in a ΛCDM cosmology renormalized with the σ_8 value of the simulations with a massive neutrino component (blue dotted lines). This means that, if an error of ~ 10 per cent is assumed on bias measurements, we are not able to distinguish the effect of massive neutrinos on β when the two cosmological models with and without ν are normalized to the same σ_8.

In Fig. 8 we show, as a function of M_ν and z, the relative difference between the theoretical β values calculated in the ΛCDM+ν and ΛCDM cosmologies, normalized to the same σ_8. At $z = 1$ and for $M_\nu > 0.6$ eV, the relative difference with respect to the $M_\nu = 0$ case is $\Delta\beta/\beta \gtrsim 3$ per cent. This result is interesting, since future spectroscopic galaxy surveys, as *Euclid*, *JEDI* and *WFIRST*, should be able to measure the linear RSD parameter with errors ≤ 3 per cent at $z \leq 1$, per redshift bin.

5 CONCLUSIONS

In this work we have studied the effect of cosmological neutrinos on the DM halo MF, clustering properties and RSD. To this purpose we have exploited the grid implementation of the hydrodynamical N-body simulations developed by Viel et al. (2010), which include a massive neutrino component, taking into account the effect of neutrinos free-streaming on the cosmic structure evolution. In order to model RSD, we have adopted the so-called streaming model (Peebles 1980), which consists of linear theory and a convolution on
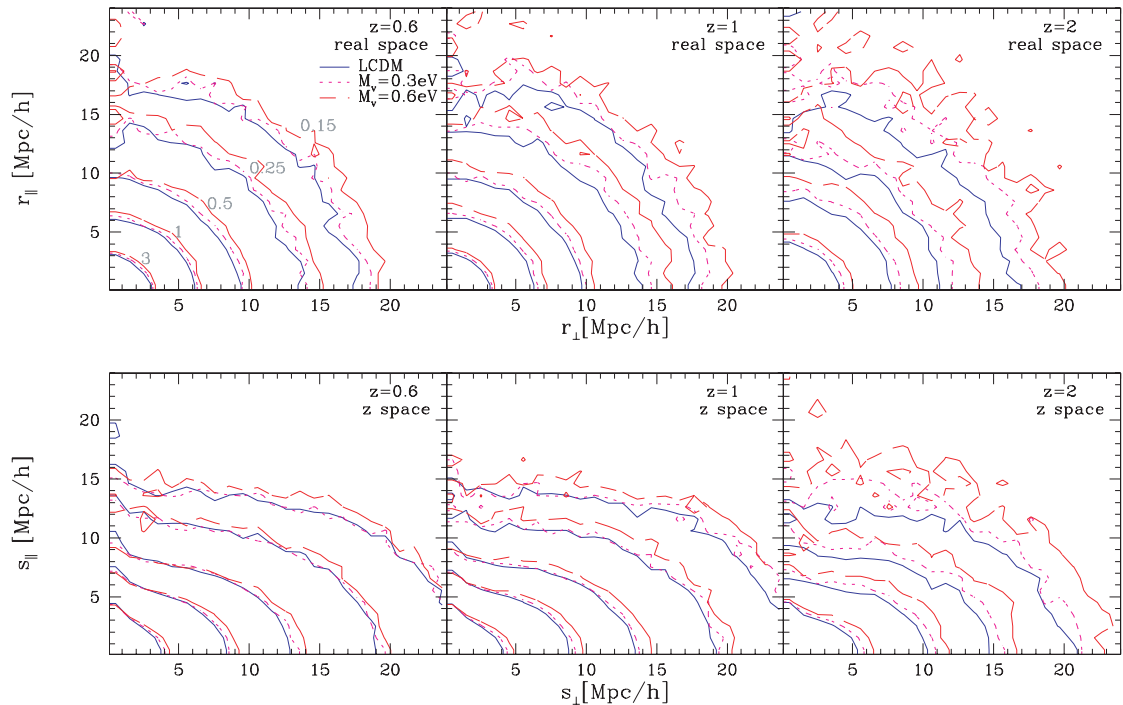

Figure 6. Two-point autocorrelation function, ξ, in real and redshift space. The contours represent lines of constant correlation, $\xi(r_\perp, r_\parallel) = 0.15, 0.25, 0.5, 1,$ 3, for $M_\nu = 0$ (blue), $M_\nu = 0.3$ eV (magenta) and $M_\nu = 0.6$ (red), respectively. Different panels show the results at redshifts $z = 0.6, 1, 2$, as labelled.
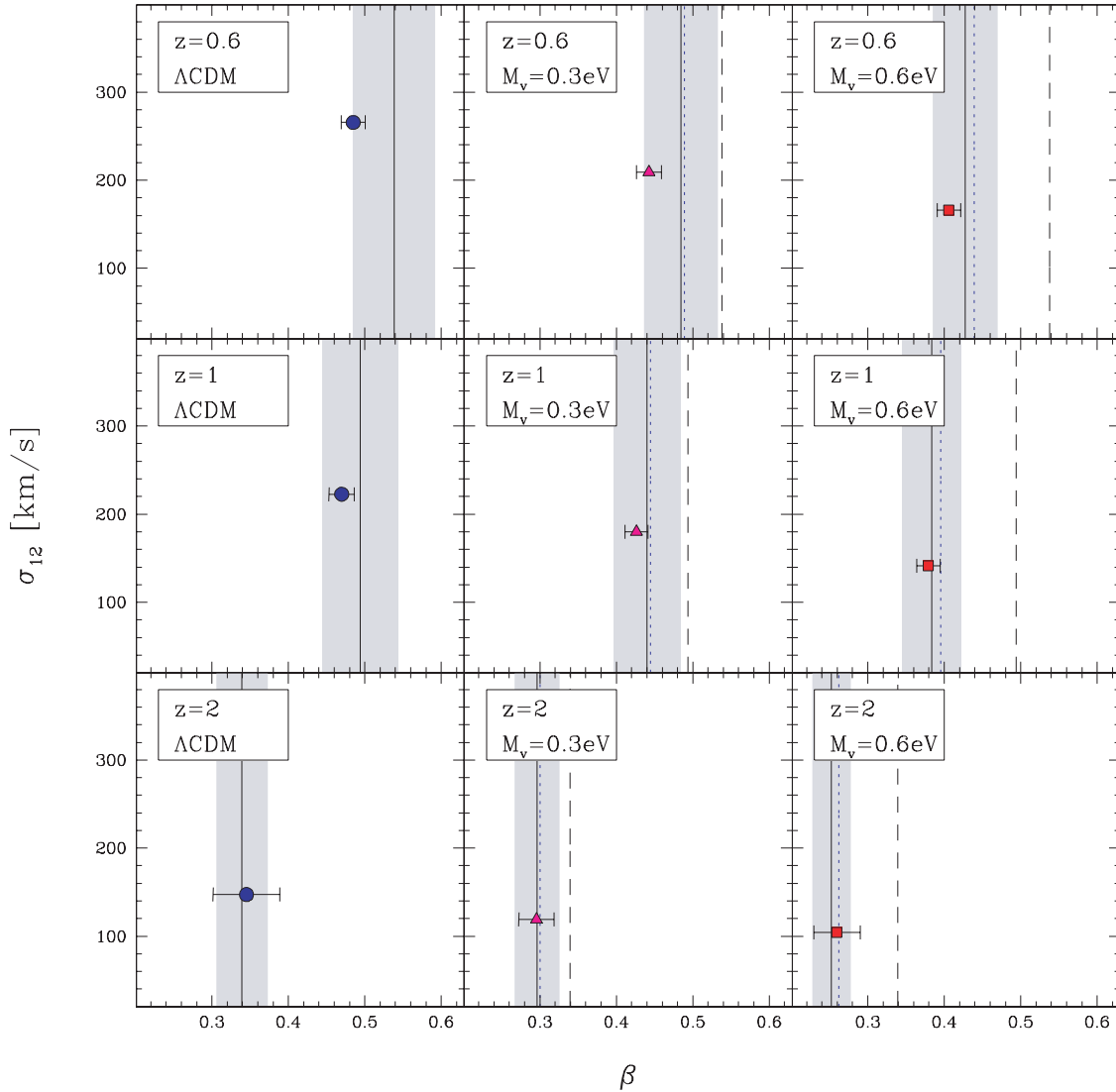
© 2011 The Authors, MNRAS **418**, 346–356
Monthly Notices of the Royal Astronomical Society © 2011 RAS

Figure 7. Best-fitting values of $\beta\sigma_{12}$, as a function of M_ν and redshift (points), compared with the ST theoretical predictions (solid lines). The dashed lines show the theoretical predictions in a ΛCDM cosmology with the same $\Delta^2_{\mathcal{R}}(k_0)$. The blue dotted lines show instead the theoretical predictions for a ΛCDM cosmology normalized to the σ_8 value of the simulation with a massive neutrino component, as explained in the text. The shaded grey bands represent the propagated $\sim$10 per cent theoretical bias error. The error bars represent the scatter in the measured β obtained dividing the simulation box in 27 sub-boxes, and rescaled by the square root of the total volume of the simulation box (Guzzo et al. 2008).

the line of sight with a velocity distribution. This model is accurate enough to robustly constrain the effect of massive neutrinos on RSD when applied on scales $\lesssim 50 \, h^{-1}$ Mpc.

We have compared the findings from the ΛCDM and the ΛCDM+ν simulations, and analysed their agreement with the analytical predictions of ST (Sheth et al. 2001; Sheth & Tormen 2002). Concerning the halo MF, we recover what is theoretically expected, i.e. starting from the same $\Delta^2_{\mathcal{R}}(k_0)$ as initial condition, massive neutrinos suppress the comoving number density of DM haloes by an amount that increases with the total neutrino mass M_ν. The suppression affects mainly haloes of mass $10^{14} < M < 10^{15} \, \mathrm{M}_\odot \, h^{-1}$, depending slightly on the redshift z. As an example, the number density of haloes with mass $10^{14} \, \mathrm{M}_\odot \, h^{-1}$ at $z = 0$ decreases by $\sim$15 per cent for $M_\nu = 0.3$ eV and by $\sim$30 per cent for $M_\nu = 0.6$ eV, and, at $z = 1$, by $\sim$40 and $\sim$70 per cent, respectively. Moreover, with increasing z, the suppression of the halo number density due to free-streaming neutrinos moves towards masses $M \leq 10^{14} \, \mathrm{M}_\odot \, h^{-1}$.

With regard to the halo clustering in the real-space, we observe that the trend of the halo correlation function $\xi(r)$ is opposite to the dark matter one. In fact, on one side, for a fixed $\Delta^2_{\mathcal{R}}(k_0)$ the total matter correlation function decreases with respect to the ΛCDM case due to neutrino free-streaming, in particular on small scales. On the other side, the halo correlation function undergoes the opposite trend since the halo bias results to be significantly enhanced. For $M_\nu = 0.6$ eV, we find that the halo correlation function in the presence of massive neutrinos at $z = 1$ is $\sim$20 per cent larger than in a pure ΛCDM model, and at $z = 2$ this difference rises up to $\sim$40 per cent. Also in this case, the theoretical ST bias model reproduces correctly the numerical findings, inside the statistical errors, and, as in the ΛCDM cosmology, the halo bias results to be scale-independent on scales larger than $r \gtrsim 20 \, h^{-1}$ Mpc.

Considering RSD, we find that the rise of the spatial halo clustering due to massive neutrinos is less enhanced in the redshift space than in the real space. In fact, on large scales, the value assumed by
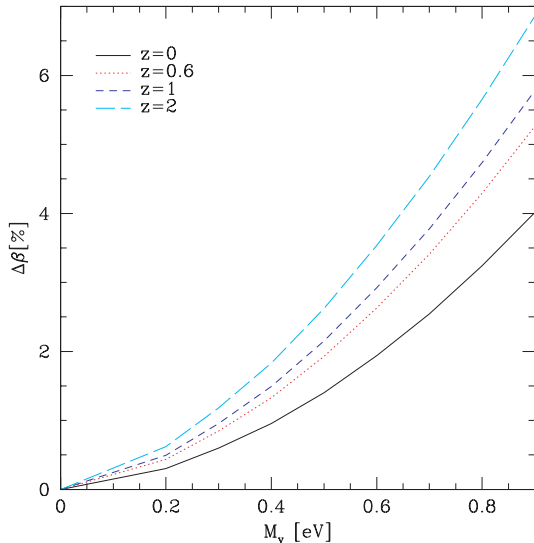
Figure 8. The relative difference between the theoretical β values calculated in the ΛCDM+ν and ΛCDM cosmologies, normalized to the same σ_8.

the bulk flow, $\langle v^2(R_*)\rangle$, in a ΛCDM+ν cosmology is smaller than in a pure ΛCDM one. On small scales, also FoG get decreased in the presence of massive neutrinos, so that the best-fitting values of β and σ_{12} reduce by an amount which increases with M_ν and z. As an example, fixed the same initial condition on $\Delta^2_{\mathcal{R}}(k_0)$, at $z = 0.6$ the β best-fitting values decrease by $\sim$10 per cent for $M_\nu = 0.3$ eV, and by $\sim$25 per cent for $M_\nu = 0.6$ eV. Likewise, the σ_{12} best-fitting values decrease by $\sim$25 per cent for $M_\nu = 0.3$ eV, and by $\sim$45 per cent for $M_\nu = 0.6$.

If not taken correctly into account, these effects could lead to a potentially fake signatures of modified gravity. Moreover, estimates of β and σ_{12} can be used to extract measurements of the total neutrino mass and may help breaking degeneracies with the other cosmological parameters.

However, these effects are nearly perfectly degenerate with the overall amplitude of the matter power spectrum as characterized by σ_8. This strong M_ν–σ_8 degeneracy undermines the potentiality of the mentioned methods in constraining the neutrino mass. For instance, the difference between the halo MFs in the ΛCDM+ν and ΛCDM models largely decreases if we normalize the two cosmologies to the same σ_8. Similarly, when analysing RSD, we find that the β best-fitting values fall in the shaded grey bands of Fig. 7, representing the propagated $\sim$10 per cent theoretical bias error, and which contain the theoretical predictions obtained in a ΛCDM cosmology renormalized with the σ_8 value of the simulations with a massive neutrino component. For such a value of the bias error, we are prevented to distinguish the effect of massive neutrinos on β, if we use as initial condition the same σ_8 value both for the ΛCDM+ν and ΛCDM cosmologies.

None the less, the σ_8 renormalization of the matter power spectrum does not totally cancel the neutrino effects which, in this case, depending on the M_ν value, alter the MF shape and amplitude especially for the less massive objects. As an example, at $z = 0$ the difference between the halo MFs with and without massive neutrinos is $\sim$3 per cent at $M = 10^{13}$ M$_\odot$ h^{-1} for $M_\nu = 0.6$ eV. The detection of this small effect depends on the sensitivity in measuring the halo MF at masses $M < 10^{14}$ M$_\odot$ h^{-1}.

More promising are measurements of β. In Fig. 8 we show, as a function of M_ν and z, the relative difference between the theoretical

β values calculated in the ΛCDM+ν and ΛCDM cosmologies, normalized to the same σ_8. At $z = 1$ and for $M_\nu > 0.6$ eV, the relative difference with respect to the $M_\nu = 0$ case is $\Delta\beta/\beta \gtrsim 3$ per cent. This results is interesting, since future nearly all-sky spectroscopic galaxy surveys, like *Euclid*, *JEDI* and *WFIRST*, should be able to measure the linear RSD parameter with errors $\lesssim$3 per cent at $z \leq 1$, per redshift bin. This means that, even exploiting information from β measurements alone, they will contribute, along with other cosmological probes, to constrain the value of the total mass of cosmological neutrinos.

ACKNOWLEDGMENTS

REFERENCES

Abazajian K., Switzer E. R., Dodelson S., Heitmann K., Habib S., 2005, Phys. Rev. D, 71, 043507
Abazajian K. N. et al., 2011, arXiv:1103.5083
Abell P. A. et al. (LSST Science Collaborations), 2009, arXiv:0912.0201
Alcock C., Paczynski B., 1979, Nat, 281, 358
Brandbyge J., Hannestad S., 2009, J. Cosmol. Astropart. Phys., 5, 2
Brandbyge J., Hannestad S., 2010, J. Cosmol. Astropart. Phys., 1, 21
Brandbyge J., Hannestad S., Haugbølle T., Wong Y. Y. Y., 2010, J. Cosmol. Astropart. Phys., 9, 14
Cabré A., Gaztañaga E., 2009a, MNRAS, 393, 1183
Cabré A., Gaztañaga E., 2009b, MNRAS, 396, 1119
Carbone C., Verde L., Wang Y., Cimatti A., 2011, J. Cosmol. Astropart. Phys., 3, 30
Doroshkevich A. G., Khlopov M. I., Sunyaev R. A., Szalay A. S., Zeldovich I. B., 1981, Ann. New York Acad. Sci., 375, 32
Elgarøy Ø., Lahav O., 2005, New J. Phys., 7, 61
Giocoli C., Tormen G., Sheth R. K., van den Bosch F. C., 2010, MNRAS, 404, 502
Giusarma E., Corsi M., Archidiacono M., de Putter R., Melchiorri A., Mena O., Pandolfi S., 2011, Phys. Rev. D, 83, 115023
Gonzalez-Garcia M. C., Maltoni M., Salvado J., 2010, J. High Energy Phys., 8, 117
Gonzalez-Morales A. X., Poltis R., Sherwin B. D., Verde L., 2011, e-print arXiv:1106.5052
Goobar A., Hannestad S., Mörtsell E., Tu H., 2006, J. Cosmol. Astropart. Phys., 6, 19
Gratton S., Lewis A., Efstathiou G., 2008, Phys. Rev. D, 77, 083507
Guzzo L. et al., 2008, Nat, 451, 541
Hamilton A. J. S., 1992, ApJ, 385, L5
Hamilton A. J. S., 1998, in Hamilton D., ed., Astrophysics and Space Science Library, Vol. 231, The Evolving Universe. Kluwer, Dordrecht, p. 185
Hannestad S., 2010, Progress Part. Nuclear Phys., 65, 185
Hannestad S., Wong Y. Y. Y., 2007, J. Cosmol. Astropart. Phys., 7, 4
Hatton S., Cole S., 1999, MNRAS, 310, 1137
Hawkins E. et al., 2003, MNRAS, 346, 78
Hu W., Eisenstein D. J., Tegmark M., 1998, Phys. Rev. Lett., 80, 5255
Jackson J. C., 1972, MNRAS, 156, 1p

Kaiser N., 1987, MNRAS, 227, 1

Kiakotou A., Elgarøy Ø., Lahav O., 2008, Phys. Rev. D, 77, 063005

Kitching T. D., Heavens A. F., Verde L., Serra P., Melchiorri A., 2008, Phys. Rev. D, 77, 103008

Komatsu E. et al., 2009, ApJS, 180, 330

Lahav O., Kiakotou A., Abdalla F. B., Blake C., 2010, MNRAS, 405, 168

Landy S. D., Szalay A. S., 1993, ApJ, 412, 64

Larson D. et al., 2011, ApJS, 192, 16

Lesgourgues J., Pastor S., 2006, Phys. Rep., 429, 307

Lewis A., Bridle S., 2002, Phys. Rev. D, 66, 103511

Lewis A., Challinor A., Lasenby A., 2000, ApJ, 538, 473

Matsubara T., 2004, ApJ, 615, 573

Mo H. J., Jing Y. P., Boerner G., 1992, ApJ, 392, 452

Okumura T., Jing Y. P., 2011, ApJ, 726, 5

Okumura T., Matsubara T., Eisenstein D. J., Kayo I., Hikage C., Szalay A. S., Schneider D. P., 2008, ApJ, 676, 889

Peacock J. A. et al., 2001, Nat, 410, 169

Peebles P. J. E., 1980, The Large-scale Structure of the Universe. Princeton Univ. Press, Princeton

Percival W. J., White M., 2009, MNRAS, 393, 297

Percival W. J. et al., 2004, MNRAS, 353, 1201

Perotto L., Lesgourgues J., Hannestad S., Tu H., Y Y Wong Y., 2006, J. Cosmol. Astropart. Phys., 10, 13

Press W. H., Schechter P., 1974, ApJ, 187, 425

Raccanelli A., Samushia L., Percival W. J., 2010, MNRAS, 409, 1525

Reid B. A. et al., 2010, MNRAS, 404, 60

Scoccimarro R., 2004, Phys. Rev. D, 70, 083007

Seljak U., Slosar A., McDonald P., 2006, J. Cosmol. Astropart. Phys., 10, 14

Sheth R. K., Tormen G., 2002, MNRAS, 329, 61

Sheth R. K., Mo H. J., Tormen G., 2001, MNRAS, 323, 1

Simpson F., Jackson B., Peacock J. A., 2011, MNRAS, 411, 1053

Smith R. E. et al., 2003, MNRAS, 341, 1311

Song Y., Percival W. J., 2009, J. Cosmol. Astropart. Phys., 10, 4

Springel V., 2005, MNRAS, 364, 1105

Springel V., White S. D. M., Tormen G., Kauffmann G., 2001, MNRAS, 328, 726

Takada M., Komatsu E., Futamase T., 2006, Phys. Rev. D, 73, 083520

Taruya A., Nishimichi T., Saito S., 2010, Phys. Rev. D, 82, 063522

Tegmark M. et al., 2004, ApJ, 606, 702

Tegmark M. et al., 2006, Phys. Rev. D, 74, 123507

Thomas S. A., Abdalla F. B., Lahav O., 2010, Phys. Rev. Lett., 105, 031301

Tinker J. L., 2007, MNRAS, 374, 477

Tinker J. L., Weinberg D. H., Zheng Z., 2006, MNRAS, 368, 85

Tocchini-Valentini D., Barnard M., Bennett C. L., Szalay A. S., 2011, ApJ, submitted (arXiv:1101.2608)

Viel M., Haehnelt M. G., Springel V., 2010, J. Cosmol. Astropart. Phys., 6, 15

Vikhlinin A. et al., 2009, ApJ, 692, 1060

Wang S., Haiman Z., Hu W., Khoury J., May M., 2005, Phys. Rev. Lett., 95, 011302

Zehavi I. et al., 2005, ApJ, 621, 22

This paper has been typeset from a T<small>E</small>X/L<small>A</small>T<small>E</small>X file prepared by the author.